JOURNAL OF GEOPHYSICAL RESEARCH, VOL. 115, D11206, doi:10.1029/2009JD012626, 2010

Soluble mass, hygroscopic growth, and droplet activation of coated soot particles during LACIS Experiment in November (LExNo)

S. Henning,[1] H. Wex,[1] T. Hennig,[1,2] A. Kiselev,[1] J. R. Snider,[3] D. Rose,[4] U. Dusek,[4,5] G. P. Frank,[4,6] U. Pöschl,[4] A. Kristensson,[6,7] M. Bilde,[7] R. Tillmann,[8] A. Kiendler-Scharr,[8] T. F. Mentel,[8] S. Walter,[9] J. Schneider,[9] C. Wennrich,[1] and F. Stratmann[1]

Received 10 June 2009; revised 15 January 2010; accepted 25 January 2010; published 4 June 2010.

[1] The LACIS Experiment in November (LExNo) campaign was conducted in November 2005 at the Atmospheric Composition Change the European Network of Excellence (ACCENT) site Leipzig Aerosol Cloud Interaction Simulator (LACIS). The goal of LExNo was to provide deeper insight into the activation properties of coated soot particles imitating aged combustion aerosol particles. The aerosols were prepared by starting with spark-generated soot particles. In some experiments the soot particles were compacted by exposure to propanol vapor; in others this step was bypassed. The soot was thermally coated with ammonium sulfate, levoglucosan, or a mixture of both ammonium sulfate and levoglucosan. The synthesized particles were investigated using aerosol mass spectrometry, a Hygroscopicity Tandem differential mobility analyzer, two Wyoming static diffusion cloud condensation nuclei (CCN) instruments, a Droplet Measurement Technologies continuous flow CCN instrument, and LACIS. A close correlation between the hygroscopic growth factor at 98% relative humidity and the critical supersaturation of CCN activation was observed. Closure between hygroscopic growth, CCN activation, and chemical composition of the investigated particles was achieved with two different single-parameter Köhler model approaches and with a third approach, a standard Köhler model using as input parameter the soluble mass as determined by aerosol mass spectrometry.

Citation: Henning, S., et al. (2010), Soluble mass, hygroscopic growth, and droplet activation of coated soot particles during LACIS Experiment in November (LExNo), *J. Geophys. Res.*, *115*, D11206, doi:10.1029/2009JD012626.

1. Introduction

[2] Biomass burning represents an important source of atmospheric aerosols and greenhouse gases. The annual globally burned area is in the range of 3 to 3.5 million square kilometers, resulting in emissions of 2.5 10^9 kgC per year [*Schultz et al.*, 2008; *van der Werf et al.*, 2006]. Soot particles themselves are known to be mainly hydrophobic, but reactions with inorganic atmospheric species can alter hygroscopic properties significantly [*Dinar et al.*, 2006; *Semeniuk et al.*, 2007; *Zhang et al.*, 2008]. Combustion aerosol particles can thereby become available as CCN and can influence climate directly by reflection and absorption of solar radiation, and also indirectly through cloud formation and rain suppression [*Albrecht*, 1989].

[3] In the Amazon Basin, for example, the CCN concentration in the dry season is an order of magnitude higher than in the wet season due to biomass burning. According to model calculations, this can lead to strongly enhanced cloud droplet number concentrations, reduced cloud droplet radii, and negative radiative forcing [*Roberts et al.*, 2003]. Variations in the size distribution and chemical composition can strongly influence the activation and growth of CCN [*Roberts et al.*, 2003].

[4] The particle concentration resulting from combustion processes is very high, but it is reduced rapidly by nonlinear processes outside the flames. Vapor condenses on the particles as the plume cools down, and the particles' ability to act as CCN increases with aging time [*Andreae and Merlet*, 2001]. Moreover, soot particles from combustion processes are modified by chemical reactions, condensation (e.g., H_2SO_4), or coagulation during long-range transport and

[1]Institute for Tropospheric Research, Department of Physics, Leipzig, Germany.
[2]Now at Institute for Applied Environmental Science, Stockholm University, Stockholm, Sweden.
[3]Department of Atmospheric Science, University of Wyoming, Laramie, Wyoming, USA.
[4]Biogeochemistry Department, Max Planck Institute for Chemistry, Mainz, Germany.
[5]Now at Institute for Marine and Atmospheric Research, Utrecht University, Utrecht, Netherlands.
[6]Now at Department of Physics, Lund University, Lund, Sweden.
[7]Department of Chemistry, University of Copenhagen, Copenhagen, Denmark.
[8]ICG-II: Troposphere, Juelich Research Centre, Juelich, Germany.
[9]Particle Chemistry Department, Max Planck Institute for Chemistry, Mainz, Germany.

0148-0227/10/2009JD012626

appear in the atmosphere as internally mixed particles. If these particles contain a soluble fraction they can efficiently act as CCN [*Dusek et al.*, 2006; *Novakov and Corrigan*, 1996].

[5] In general the interaction between aerosol and cloud droplet number concentration can be very complex. Recent model calculations have found that an enhanced aerosol number can either result in an increase or reduction of cloud droplet number depending on the ratio between smoke and general pollution particles [*Lee et al.*, 2006].

[6] Several aerosol-CCN closure studies have been performed on atmospheric particles to elucidate the relation between particle properties and the concentration of cloud droplets. These closure studies exhibit still unresolved biases, even though the models account for the the most important particle components and consider the dominant processes [*Stroud et al.*, 2007; *Vestin et al.*, 2007].

[7] Aged soot particles become not only available as CCN, but the enhanced hygroscopic growth due to a gained coating will also alter the optical properties of the soot. For example, *Zhang et al.* [2008] found an increase in scattering by about a factor of 10 and in absorption by nearly a factor of 2 at 80% RH for soot particles treated with sulfuric acid vapor relative to fresh soot particles.

[8] The LExNo laboratory experiment was designed to minimize the factors that complicate aerosol-CCN closure under atmospheric conditions, but still work on a near-realistic wood combustion aerosol. For this reason a coating was applied to synthesized soot particles to simulate the aging process of the particles in the atmosphere.

[9] Two types of coating material were chosen: The first coating material was levoglucosan, which is known to be a substantial constituent of wood combustion aerosol [*Andreae and Merlet*, 2001], and is used as a tracer for wood combustion particles. The second coating material was ammonium sulfate, which turned out to be present after heating as either ammonium sulfate or ammonium hydrogen sulfate. Ammonium and sulfate are known to be abundant in the atmospheric aerosol and are thereby useful model substances for the soluble particle fraction. Ammonium hydrogen sulfate has been used previously in other experiments to model the amount of soluble material in smoke particles [*Roberts et al.*, 2003]. Both substances, levoglucosan and ammonium sulfate, are known to be hygroscopic with growth factors of about 1.35 and 1.7, respectively, for a dry diameter of 100 nm at 90% RH [e.g., *Koehler et al.*, 2006; *Petters and Kreidenweis*, 2007] and the coatings are thus expected to enhance the CCN activity of soot significantly.

[10] Our study shows that closure can be achieved between hygroscopic growth, droplet activation, and chemical composition of the investigated particles, by applying (1) single-parameter Köhler model approaches and (2) a standard Köhler model using the number of soluble moles of coating derived by aerosol mass spectrometry as input parameter.

2. Experimental Setup

[11] A detailed description of the LExNo experiment is given in the overview paper by *Stratmann et al.* [2010]. Here a brief description of the features relevant for the hygroscopicity and activation measurements is given. The particles studied consisted of a soot core and a coating. Two particle characteristics were varied during the course of the experiments: (1) the structure of the soot core and (2) coating substance.

[12] As described by *Stratmann et al.* [2010] the experiments were done on soot particles produced by a graphite aerosol generator (GfG-1000, PALAS®, Germany). These particles are known to have a complex, nonspherical, shape [*Mikhailov et al.*, 2001; *Wentzel et al.*, 2003]. In some of the experiments, the structure of the soot particles was changed by compacting them with propanol [*Kütz*, 1994]. For this the particles were passed over a pool of liquid 2-propanol (in the following labeled: pcs standing for propanol-compacted soot). Downstream of the reservoir the 2-propanol vapor was removed from the carrier gas together with some of the propanol bound to the particles by an annular diffusion dryer filled with activated charcoal. If no compaction was desired, the propanol compaction unit was bypassed (ucs, uncompacted soot).

[13] The soot cores were size selected by a DMA (differential mobility analyzer). Different coatings were applied by means of furnaces to the size-selected pcs or ucs cores. An ammonium hydrogen sulfate (AHS) or an ammonium sulfate (AS) coating was produced by heating AS to temperatures between 93°C to 170°C. Levoglucosan (LG) coating was applied by heating LG to temperature between 80°C and 106°C (for details see *Stratmann et al.* [2010]).

[14] Using a second DMA the particle electromobility diameter was held constant at 84 nm for the experiments discussed, and the hygroscopic mass per particle in the coatings was varied by the coating temperature of the furnaces. Size distribution measurements [*Stratmann et al.*, 2010] after the coating, before the second DMA, showed that the maximum of the number size distribution was at 84 nm and that the fraction of doubly charged particles was on the order of 1%, thus we neglected multiple-charged particles for the experiments with coated soot. The mass of the coating was monitored with two Quadrupole Aerosol Mass Spectrometers (Q-AMS, Aerodyne Research) instruments [*Canagaratna et al.*, 2007; *Jayne et al.*, 2000]. The AMS is capable of detecting components which are volatile at temperatures smaller than 600°C; this is the case for LG, AS and AHS but not for soot [*Schneider et al.*, 2006]. The composition of the coatings was analyzed in terms of ammonium, sulfate, and total organics as described by *Allan et al.* [2003]. The data sets of the two AMS instruments were compared and showed very good agreement. The data used here result from a merged data set from both instruments.

[15] As expected, when the temperature of the coating furnaces was increased, more coating was found on the soot cores (Figure 1). Figure 1 seems to suggest that the total applied mass in the LG coating experiments is dependent on the core type. The pcs (solid symbols) receive the same amount of LG coating at lower coating temperatures than ucs (open symbols) for soot cores of the same mobility-equivalent size. The experiments were however performed on different days with different batches of LG and thus we cannot draw firm conclusions regarding the amount of LG on different core types. The mass of AS was not sensitive to the character of the soot core.

[16] The AMS measurements deliver the mass concentrations for ammonium and sulfate in a straightforward

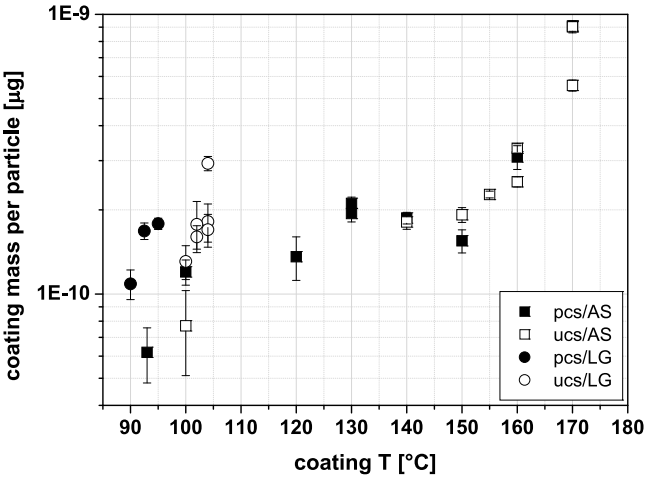

Figure 1. Mass of AS or LG on coated soot particles (electomobility d_{dry} = 84 nm) versus temperature of the coating furnace. Solid symbols indicate soot particles that were compacted with propanol prior to coating (pcs), and open symbols indicate uncompacted soot (ucs).

manner. For the coatings generated by AS, the analysis of the coating composition revealed that the molar ratio of ammonium to sulfate was only around 1.1 (±10%): This is equivalent to a deficit of about one ammonium per sulfate leading to the conclusion that the particle coating consisted of AHS.

[17] The same analysis by AMS measurements of AS particles prepared by atomizing and drying aqueous solutions yielded the expected molar ratio of 2 (2.2 ± 10%) for AS, which supports the above analysis of NH_4 loss. In the literature, thermal decomposition of AS is only reported for temperatures higher than 170°C [e.g., *Halstead*, 1970; *Kiyoura and Urano*, 1970], but it seems that this process is taking place at lower temperatures during the coating procedure in our experiments. Figure 2 shows the ammonium-to-sulfate molar ratio (n_{NH4}/n_{SO4}) plotted versus the coating temperature of the furnace. For particles coated with AS and LG the molar ratio of ammonium to sulfate was higher 1.8 (±10%) leading to the conclusion that here the coating mainly consists of AS.

[18] In the case of the AHS-coated particles, evidence for significant amounts of organics was detected in the AMS mass spectra. This mass spectrometric signature was observed, independently if the core of the AHS-coated particles was compacted with propanol or not. The mass spectroscopic pattern of the organic component was reconcilable with that of propanol, as measured by AMS in a lab experiment. It is not clear why there is propanol also in the uncompacted case. In the following soot particles that passed through the AS furnace are designated as being coated with AHS and propanol (AHSp).

[19] In the AMS spectra from the LG coating negligible propanol signature (1–4% of the total organic mass) was found as could be demonstrated by the following procedure. We made use of the fact that LG has a signal at m/z = 60 which is a unique marker for carbohydrates (sugars). This m/z = 60 is absent for bare soot (pcs and ucs) and in particles with AHS and propanol coating. The propanol component has a significant signal at m/z = 45. The signal m/z = 45 can be observed in pure LG and in LG-coated soot particles, but is minor. The signals at m/z 60 and m/z = 45 appear in the same fixed ratio for both cases leaving no room for a propanol component in the LG coatings. This is somewhat surprising, as the setup with exception of the LG furnace was identical for both particle types. This finding indicates that some kind of specific interaction might take place between AS and propanol, which is not relevant for LG. We also applied the analysis using the signals at m/z = 60 and m/z = 45 to the mixed coatings. Coatings with AS and LG show a clear propanol signature in the AMS spectra.

[20] Hygroscopic particle growth of the generated particles up to 98% RH was examined with a High Humidity Tandem Differential Mobility Analyzer (HH-TDMA) [*Hennig et al.*, 2005]. For the investigation of the critical supersaturation two cloud chamber types were utilized: two Wyoming static diffusion cloud condensation nuclei (CCN) instruments [*Snider et al.*, 2006], a continuous flow CCN instrument (DMT-CCNC) [*Roberts and Nenes*, 2005], [*Rose et al.*, 2008] and the Leipzig Aerosol and Cloud Interaction Simulator (LACIS) [*Stratmann et al.*, 2004; *Wex et al.*, 2006]. For results concerning the intercomparison of these instruments, see *Snider et al.* [2010]. Throughout this paper the critical supersaturation values determined with the DMT-CCNC have been used for further analysis, as this data set was the most complete. The instrument was calibrated with AS aerosol [*Rose et al.*, 2008] by applying a composition-dependent water activity parameterization. For ammonium sulfate molalities less than 0.8 mol/kg the water activity parameterization of *Young and Warren* [1992, equations (8) and (11)] was applied, and for molalities larger than 0.8 mol/kg a fit of the water activity data presented by *Low* [1969] was applied (Table 1).

[21] Monodisperse particles consisting of pure AS or pure LG, which were used for calibration purposes and in case of pure LG also for activation analysis (see section 4.1.2), were prepared by atomizing an aqueous solution of AS or LG, followed by drying and size selection of the particles. In case of the pure LG particles an enhanced proportion of multiple-charged particles was observed [cf. *Stratmann et*

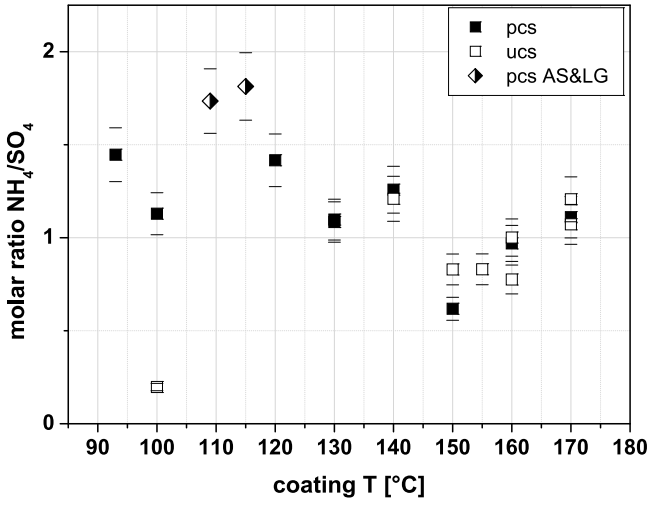

Figure 2. Dependency of coating composition on furnace temperature. The molar ratio of NH_4/SO_4 should be 2 for AS and 1 for AHS (error bars: 10% error in mass).

Table 1. Properties of Compounds Used for Particles Coatings in Köhler Theory: Molar Mass, Density, and van't Hoff Factor[a]

	M (kg/mol)	ρ (kg/m^3)	v
Ammonium	0.018		
Sulfate	0.096		
$(NH_4)_2SO_4$	0.132	1770	x[b]
NH_4HSO_4	0.115	1780	2
Propanol	0.060	803.5	1
Levoglucosan	0.162	1618[c]	1

[a]M, molar mass; ρ, density; v, van't Hoff Factor.
[b]For AS molalities smaller than 0.8 mol/kg the parameterization of *Young and Warren* [1992, equations (8) and (11)] was applied. For molalities larger than 0.8 mol/kg a fit of the water activity data published by *Low* [1969] was applied.
[c]*Park et al.* [1971].

al., 2010; *Kiselev et al.*, 2010] and the AMS data have been corrected for this.

3. Data Modeling

[22] The vapor pressure p of water over an aqueous solution droplet relative to that over a flat water surface p_0 is given by the Köhler equation [*Köhler*, 1936],

$$\frac{p}{p_0} = s = a_w \exp\left(\frac{4\sigma M_w}{RT\rho_w d_{wet}}\right) \quad \text{with} \quad S = (s-1)*100\%, \qquad (1)$$

where s is saturation, a_w is the water activity, d_{wet} is the droplet diameter, M_w is the molar mass of water, ρ_w is the density of water, σ is the air-liquid surface tension, R is the gas constant, T the temperature and S supersaturation. The critical supersaturation is the maximum in a plot of S versus d_{wet}.

[23] For a solution droplet containing i soluble species the water activity can be expressed as

$$a_w = \frac{n_w}{n_w + \sum_i v_i n_i}, \qquad (2)$$

where v_i is the van't Hoff factor, which is a measure for the degree of dissociation of the soluble material, n_i is the number of moles of compound i.

[24] Assuming volume additivity the number of moles of water n_w can be calculated via the wet and dry particle diameters, d_{wet} and d_{dry}, respectively.

$$\text{with} \quad n_w = \frac{\rho_w}{M_w}\frac{\pi}{6}\left(d_{wet}^3 - d_{dry}^3\right). \qquad (3)$$

This equation is also valid for particles containing an insoluble core, when the total dry particle diameter d_{dry} includes core and soluble material. All calculations were done assuming spherical particles, a surface tension of water σ = 72.8 mN/m and a temperature of 20°C.

[25] To achieve closure between subsaturated and supersaturated measurements different approaches for the determination of a_w were applied and are presented in sections 3.1 and 3.2.

3.1. Modeling Based On Observed Coating Mass

[26] If particle properties such as density and molar mass are available the critical supersaturation S_c can be explicitly calculated applying equation (1) to (3). For the measurements presented here this was possible as the properties of the solute were known (see Table 1) and the mass of solute on the particles was determined by the AMS measurements. The masses as measured with the AMS were divided by the measured total particle number (measured with a Condensation Particle Counter, CPC-3025, TSI), which yields the average mass per particle for all species j (m_j) with j representing LG, propanol, sulfate or ammonium. From m_j the number of moles of species n_j was calculated $n_j = \frac{m_j}{M_j}$, with M_j molar mass of species j (see Table 1).

[27] However, for the calculation of the water activity following equation (2) the number of moles per compound n_i are needed with i representing LG, propanol, AS or AHS. For LG and Propanol n_j is equal to n_i, because the stoichiometric coefficient is unity. For the species ammonium and sulfate we assumed that either all sulfate was present as AS or as AHS, which are the limiting cases. The number of moles per compound n_i for AS and AHS can than be deduced from n_j for sulfate, considering that for each mole of sulfate one mole of AS/AHS is present. Inserting the respective n_i into equation (2) and applying equation (1) gives the Köhler curve for a dry particle diameter d_{dry} considering the respective soluble mass of sulfate, propanol, or levoglucosan as measured with AMS, with the remaining fraction of the particle being insoluble. In this approach, nonideality is taken into account in equation (2) through the use of v_i as given in Table 1.

[28] For illustrative reasons (see Figure 3 and 4), also the total number of moles of soluble species n_{tot} per particle was calculated from the AMS measurements as follows:

$$n_{tot} = \sum_j n_j. \qquad (4)$$

In an ideal solution n_{tot} would be the total number of moles in solution.

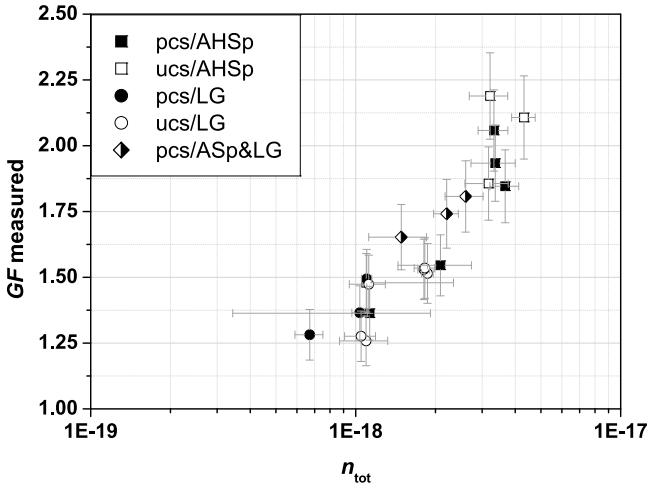

Figure 3. Overview of the hygroscopic growth factors, GF, measured in this study for coated soot particles (electromobility d_{dry} = 84 nm). GF are plotted versus the total number of moles of soluble coating material n_{tot} as determined by AMS. Horizontal error bars indicate the uncertainties of the AMS measurements, and vertical error bars indicate standard deviation of measurement data.

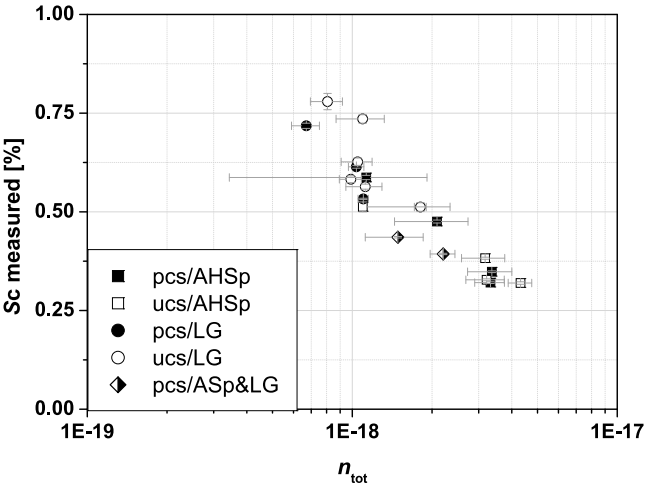

Figure 4. Overview of the critical supersaturation S_c for the CCN activation of coated soot particles with a fixed electromobility dry diameter (d_{dry} = 84 nm). S_c is shown as a function of the total number of moles n_{tot} of coating material determined by AMS. Horizontal error bars indicate the uncertainties of the AMS measurements, and vertical error bars indicate standard deviation of measurement data.

3.2. Modeling Based On One-Parameter Approaches

[29] Often the properties of the solute are not known, and a full solution of the Köhler equation is not possible. In the literature several parameterizations are discussed to handle this problem. In this study the "ρ_{ion}" parameterization [*Wex et al.*, 2007] and the "κ" parameterization [*Petters and Kreidenweis*, 2007] were applied to parameterize water activity for the dry and wet particle diameter,

$$a_w = \exp\left(-\rho_{ion}\frac{M_w}{\rho_w}\cdot\frac{d_{dry}^3}{d_{wet}^3 - d_{dry}^3}\right) \quad (5)$$

$$a_w = \frac{d_{wet}^3 - d_{dry}^3}{d_{wet}^3 - d_{dry}^3(1-\kappa)}. \quad (6)$$

The hygroscopicity parameter (ρ_{ion} or κ) from growth factor data (d_{wet}/d_{dry} versus RH) is obtained by inserting equation (5) or (6) into equation (1) and solving for ρ_{ion} or κ. For the measurements presented here, which were performed at relative humidities of about 98% (HH-TDMA) [*Hennig et al.*, 2005] we can approximate

$$\kappa \approx \rho_{ion}\frac{M_w}{\rho_w}. \quad (7)$$

[30] Both parameters were independently used to predict the critical supersaturation S_c and the results are presented in comparison with the CCN measurements from the DMT instrument in section 4.2.

4. Results

[31] The synthesized particles were investigated with respect to their hygroscopic growth factor (GF) and their critical supersaturation needed for activation (S_c). We tried to achieve closure by predicting the critical supersaturation in two ways, first from the soluble particle fraction derived by AMS and second by parameterization and extrapolation of the hygroscopic growth. In addition, the hygroscopic particle growth based on the derived soluble particle fraction was predicted and compared to the measurements.

[32] The particles' growth factor GF was calculated as d_{wet}/d_{dry} from the HH-TDMA data. If not mentioned otherwise GF is given for a dry particle diameter of 84 nm and a relative humidity of 98%.

4.1. Relationship Between Hygroscopic Growth, Activation Behavior, and Soluble Particle Fraction

4.1.1. Observation of Growth Factors and Critical Supersaturation

[33] We observed relative simple relationships between hygroscopic growth or droplet activation and number of moles of coatings n_{tot} as derived from the AMS measurements. Figure 3 presents the overview of the observed growth factors for the different particle types in relation to n_{tot} (see equation (4)). As can be seen the measured GF for a dry particle electromobility diameter of 84 nm and a relative humidity of 98% were found in a range from 1.25 to 2.25 for a range of n_{tot} between 5×10^{-19} and 5×10^{-18} mol. The horizontal error bars in Figures 3 and 4 consider the uncertainty of the AMS measurements for each species and vertical error bars indicate standard deviation of measurement data. As expected GF increase with increasing number of moles of solute. For AHSp coated soot the GF were between 1.3 and 2.25. Soot particles coated with LG did not take up as much water and their GF were between 1.25 and 1.5. The soot particles coated with both AHS and LG exhibited a GF in between with about 1.7. No influence of propanol compaction was observed in the growth factor measurements. This is attributed to observed compaction of the particles when they were coated with AHSp or LG independent from a previous compaction with propanol [cf. *Kiselev et al.*, 2010].

[34] In a similar way, Figure 4 gives the critical supersaturation S_c versus the total number of moles of coating material per particle as derived from the AMS measurements. The more soluble material is on the particles, the easier the particles were activated. The soot particles coated with AHSp activated at lower supersaturations than LG coated particles. Activation of soot coated with AHSp was observed between 0.3% and 0.6% supersaturation for a dry particle diameter of 84 nm. For soot coated with LG the critical supersaturation was observed between 0.5% and 0.75%. Propanol-compacted soot coated with LG and AHSp activated around 0.32%. As in the case of the hygroscopic growth propanol compaction of the soot showed no effect.

[35] Figures 3 and 4 show clear correlations between the total number of moles of coating material and the hygroscopic growth at 98% RH and critical supersaturation at a set dry particle diameter (electromobility d_{dry} = 84 nm). This is expected since the water activity and thus water uptake is determined by the number of moles of soluble material in the droplet as shown in equation (2). The total number of moles of coating material obtained from AMS measurements corresponds to the total number of moles of soluble material assuming ideality.

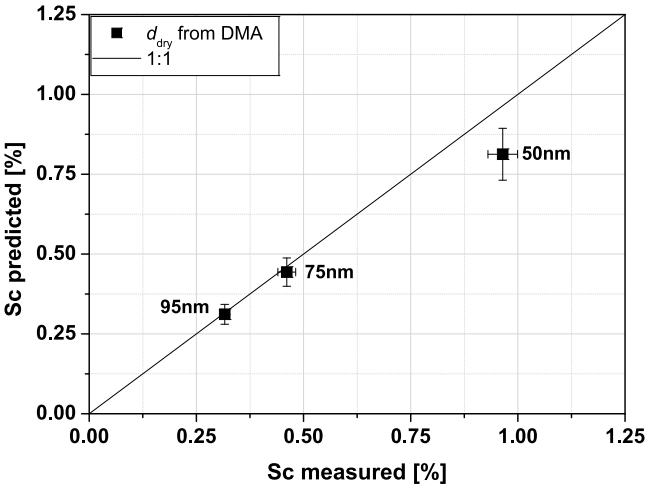

Figure 5. Predicted versus measured critical supersaturation for pure LG particles (T = 20°C, σ(T) = 72.8 mN/m) for different dry particle diameters selected with the DMA. Köhler model predictions are based on d_{dry}.

[36] The scattering of the data points around a narrow band in Figures 3 and 4 can in part be ascribed to uncertainty in n_{tot} which is attributed to AMS inherent uncertainties. Another issue is that different coatings may result in different deviations from ideality.

[37] The correlations between total number of moles of coating material and GF or S_c are pronounced and we therefore conclude that modeling based on the total number of moles of coating material obtained from AMS measurements will be possible. The modeling results for hygroscopic growth and critical supersaturation based on AMS measurements are presented for each particle type separately in section 4.

4.1.2. Modeling Hygroscopic Growth and the Critical Supersaturation Based On Soluble Mass As Measured by AMS

[38] The hygroscopic growth and critical supersaturation were calculated directly using equations (1) and (2). The number of soluble moles of sulfate and organics (levoglucosan, propanol) were used in the Köhler equation as explained in section 3.1. By applying the respective van't Hoff factors in equation (1) we accounted for the nonideality of the solutions. For comparison the predicted values are presented versus the measured values.

4.1.2.1. Particles Consisting of Pure LG

[39] For the monodisperse particles consisting of pure LG, which were prepared by atomizing an aqueous solution, drying and selecting particles, based on a mobility size, the critical supersaturation S_c was calculated in terms of the dry diameter. The diameter was used in Köhler theory (equations (1) and (2)) applying the properties for LG as given in Table 1 [*Rosenorn et al.*, 2006]. The predicted values of S_c from this analysis are shown versus the measured S_c in Figure 5.

[40] For d_{dry} taken from the DMA the measured and predicted S_c values compare well for 75 and 95 nm dry diameter. For d_{dry} = 50 nm the measured S_c is 20% higher than the predicted value. This is outside the errors limits and is not in accordance with literature data [*Rosenorn et al.*, 2006] who found activation in agreement with Köhler theory for LG. However, considering that only one measurement at this diameter is available the overall agreement between observation and prediction is satisfying.

4.1.2.2. Soot Particles Coated With LG

[41] Figure 6 compares measured GF and predictions based on the number of moles of levoglucosan in the coating as determined by AMS. Within the errors of measurement and model calculations all data points fall on the 1:1 line. The errors for both are substantial though, nevertheless the deviation of the predicted values is less than 5% in most cases and 9% at maximum. Error bars are smaller for droplet activation in Figure 7. Here using the AMS detected number of moles of levoglucosan in the coating in Köhler theory leads to an excellent agreement with the experimental data. The soot particles which were precompacted with propanol exhibit slightly lower critical supersaturations than is predicted. For the uncompacted particles no general trend was observed. The results for GF and S_c indicate that AMS measurements of a single component organic nonrefractory coating on refractory cores is feasible and leads to reliable determination of the coating amount. For levoglucosan coating the AMS combined with classical Köhler theory is a useful tool for the prediction of the critical supersaturation as well as hygroscopic growth.

4.1.2.3. Soot Particles Coated With AHSp

[42] As discussed in section 2, soot particles which were passed over the heated AS gained an AHS coating which included propanol. So we observe two components of soluble material consisting of an inorganic salt and a single organic component. Ammonium to sulfate mole ratios were around 1 for AHSp coatings but showed some variation (Figure 2). In calculations of n_{tot} this was explicitly considered. For the Köhler calculations we took the AMS derived number of moles of sulfate and considered AS and AHS as 'limiting' cases. In order to investigate if the distinction between AS and AHS is a critical issue in the study,

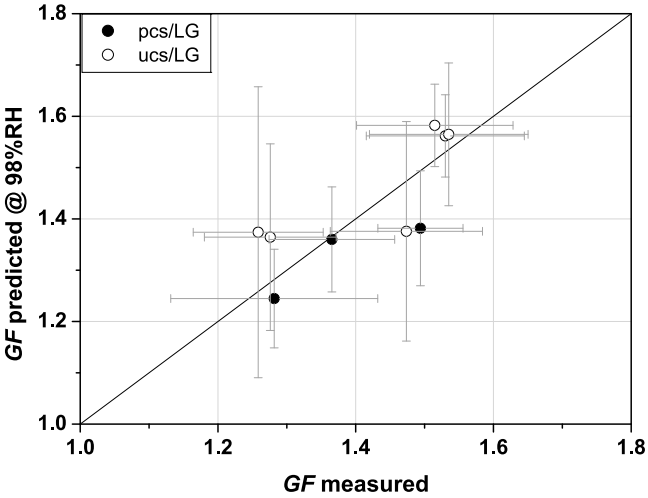

Figure 6. Predicted versus measured GF for soot particles coated with LG. Köhler model predictions are based on the number of moles of coating determined by AMS. Error bars indicate standard deviation of measurement data and are based on standard deviation of AMS measurements for predicted values.

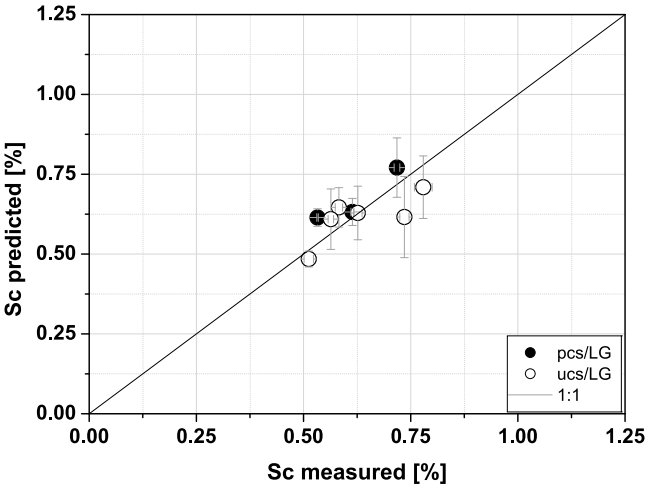

Figure 7. Predicted versus measured critical supersaturation for soot particles coated with LG. Köhler model predictions are based on the number of moles of coating determined by AMS. Error bars indicate standard deviation of measurement data and are based on standard deviation of AMS measurements for predicted values.

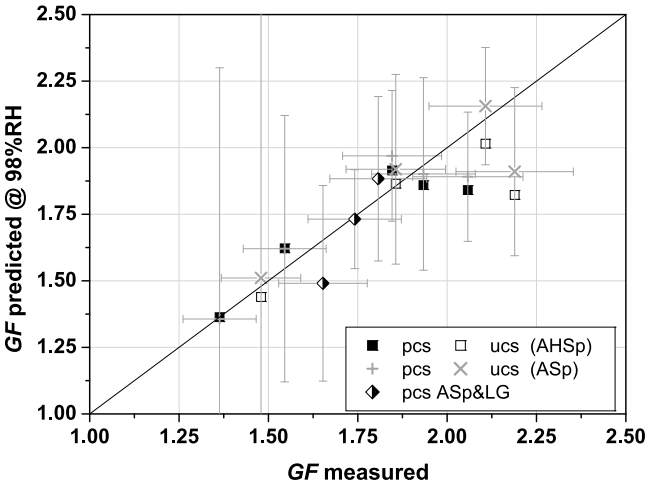

Figure 8. Predicted versus measured GF for soot particles coated with AS or AS plus LG. Köhler model predictions are based on the number of moles of soluble species in the coatings as determined by AMS assuming two different coating types (AHS + propanol and AS + propanol). Error bars indicate standard deviation of measurement data and are based on standard deviation of AMS measurements for predicted values. They are given only for AS + propanol particles to not overload the plot, but are analogous for the AHS + propanol coatings.

we performed a sensitivity study of the influence of the assumptions made regarding the properties of the coating substance on the prediction of hygroscopic growth at 98% RH and the critical supersaturation. Two scenarios were studied: (1) the number of moles of sulfate was attributed to AHS, i.e., neutralized by 1 mole NH4, and the detected organic mass to propanol; (2) the number of moles of sulfate was assumed to be present as AS, i.e., neutralized by 2 NH4, and the organic mass to be propanol. Solute properties were taken as stated in Table 1.

[43] Predicted versus measured GF for the two scenarios are shown in Figure 8 for both the propanol-compacted and the uncompacted particles. Also for the two component coatings the predicted and measured values fall on the 1:1 line within the error bars. With few exceptions, assuming ASp as coating substance led to larger predicted GF than assuming AHSp. But these differences are small compared to the error bars.

[44] Even better agreement was found between measured and predicted critical supersaturations (Figure 9). Under the assumption of AHS the number of moles is about 12% higher than under the assumption of AS, but for this is compensated by the higher van't Hoff factor of AS leading to almost the same value in critical supersaturation.

[45] The precompaction of the soot with propanol showed no systematic effect neither in predicted GF vs measured GF nor in predicted S_c versus measured S_c. This again indicates that the coating process itself obviously compacts the soot core [*Kiselev et al.*, 2010]. The good correlations between predicted and measured values in Figures 8 and 9 indicate that also for two components, a salt mixed with a organic compound, we were able to derive the coating mass and the number of moles of soluble material in coatings on refractory cores from AMS measurements.

4.1.2.4. Soot Coated With ASp and LG

[46] For the soot particles coated with AS and LG the AMS measurements showed that the ammonium to sulfate ratio is 1.8 (±10%) indicating that AS instead of AHS was present in the mixed coatings. In addition to AS and LG also propanol was detected by AMS in the mixed coatings, thus we observe a three component coating, consisting of a salt and two organic components. The AMS derived number of moles of coating was directly used in the Köhler

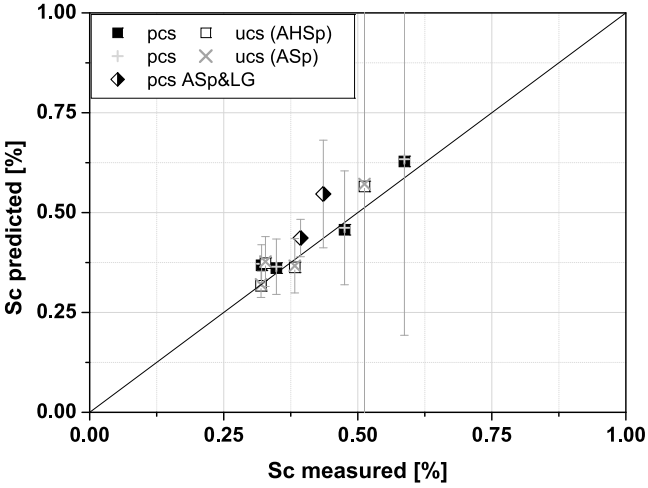

Figure 9. Predicted versus measured critical supersaturation for soot particles coated with AS or AS plus LG. Köhler model predictions are based on the number of moles of soluble species in the coatings as determined by AMS assuming two different coating types (AHS + propanol and AS + propanol). Error bars indicate standard deviation of measurement data and are based on standard deviation of AMS measurements for predicted values.

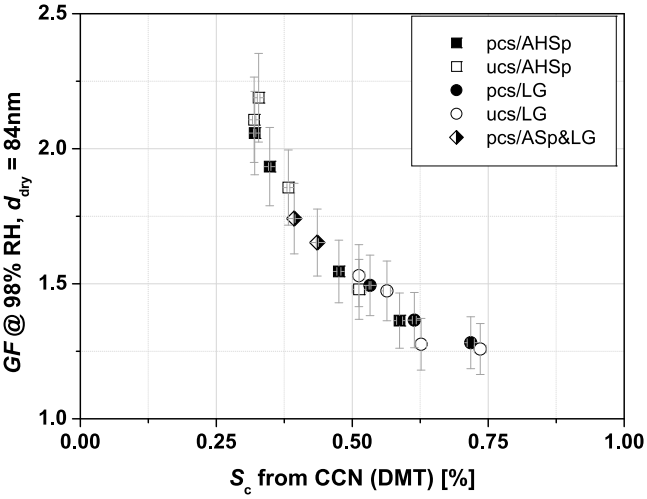

Figure 10. Relationship between growth factor at 98% RH and critical supersaturation of coated soot particles (electromobility d_{dry} = 84 nm). Error bars indicate standard deviation of measurement data.

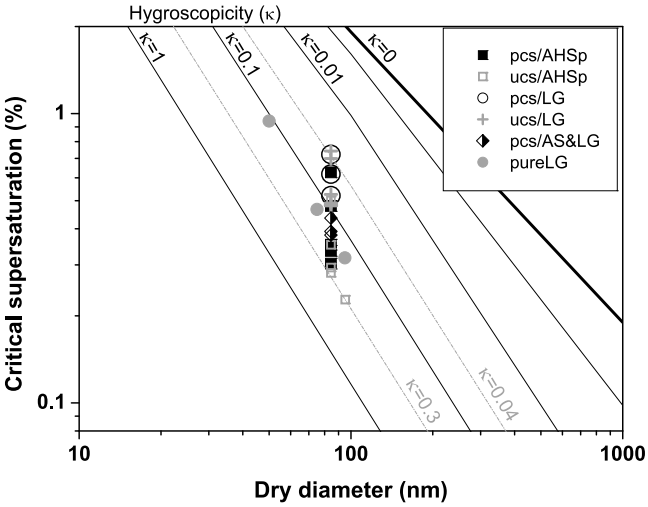

Figure 11. Critical supersaturation versus dry particle diameter for all investigated particle types: pure LG, propanol-compacted soot, and uncompacted soot with varying amounts of coating material (LG, AS, and AHS). Lines represent Köhler model predictions for different hygroscopicity parameter values in the range of $\kappa = 0$ to $\kappa = 1$.

model accounting for an insoluble core and the three components (AS, propanol, LG = ASp&LG). Predicted GF for ASp&LG are shown in Figure 8, predicted S_c were included in Figure 9.

[47] The three predicted GF of the ASp&LG coatings fall on the 1:1 line within the error bars, but for the two cases available, the critical supersaturation is slightly overestimated by 10% and 30%. The agreement for the three component coatings is satisfying considering the fact that all three masses (AS, LG, and propanol) necessary for the Köhler calculation were very small (on the order of of 1×10^{-11} μg/particle for 1×10^4 particles cm^{-3}, thus 0.1 μg/m^3) and hence close to the detection limit of the AMS. Nevertheless the approach of classical Köhler theory with AMS derived number of moles of soluble coating material appears to be applicable also for more complex mixtures of particles.

4.2. Relationship Between Hygroscopic Particle Growth and Critical Supersaturation

4.2.1. Observed Growth Factor and Critical Supersaturation

[48] Measured GF are plotted versus the measured critical supersaturation S_c in Figure 10 for a fixed particle diameter and a fixed relative humidity at the HH-TDMA of 98%. With an increase in S_c a decrease in GF was observed; that is, the more hygroscopic the particles are, the easier they activate. The trend is similar for all investigated particle types.

4.2.2. Modeling S_c Based On Hygroscopic Particle Growth

[49] As described above the hygroscopic growth factor was fitted with two different one-parameter approaches (equations (5) and (6)). In Figure 11 the critical supersaturation is plotted against the corresponding dry diameter. In most cases the diameter was 84 nm, but the particles contained varying amounts of coating material depending on the furnace temperature as described above. The plot is underlain with the "κ-value area" giving a range for the value of κ. The κ value was found to be in the range from 0.04 to 0.3. For the pure LG particles at different diameters the κ value is about constant at 0.16 which is in agreement with literature values [*Petters and Kreidenweis*, 2007]. For the soot particles coated with LG the κ value is below 0.1 and reaches 0.04 in minimum. For the AHSp coating, κ values from 0.06 to 0.3 were found.

[50] The values for ρ_{ion} (not shown) were found analogously by fitting the HH-TDMA data. The values for ρ_{ion} follow the relationship given in equation (7) and are in the range 2 to 17 kmol/m^3.

[51] The retrieved κ and ρ_{ion} values were used for the prediction of S_c. Only a slight difference in S_c between the two approaches was found, with S_c predicted via ρ_{ion} being about 1% higher for all particle types. This deviation is in

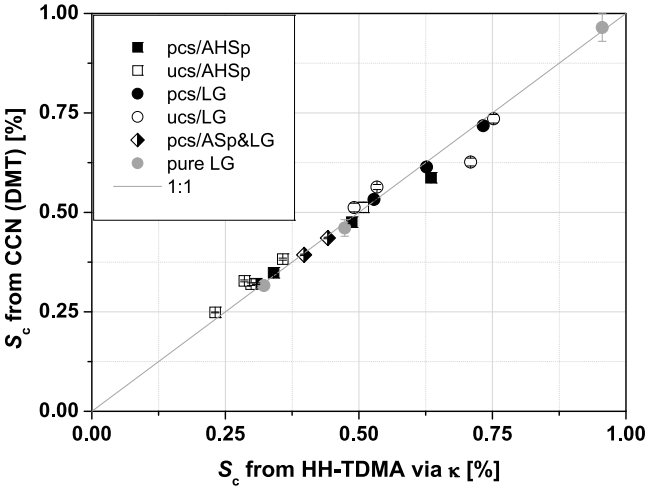

Figure 12. Critical supersaturation measured with CCN counter versus critical supersaturation predicted from HH-TDMA data using the κ-Köhler approach.

agreement with theoretically expected values for a relative humidity of 98% (M. D. Petters, personal communication, 2008) and as the deviation in the results is small, means that both approaches are equally suitable for the prediction of S_c at high relative humidities.

[52] As the difference between κ-value predicted S_c and ρ_{ion}-predicted S_c is so minimal, Figure 12 presents only the results gained via the κ-value approach. The closure between predicted and measured S_c is excellent for all synthesized particles types, suggesting that a single parameter description of hygroscopic and CCN properties is suitable for particles consisting of an insoluble core and a soluble coating.

5. Summary and Conclusion

[53] The particles generated in the laboratory, mimicking combustion products, were varied in terms of (1) the structure of the soot core before coating and (2) the applied coating. The coating consisted of AHS including propanol or LG or both. For comparison also pure LG particles were investigated. For these particle types the relationship between hygroscopicity, hygroscopic mass and critical supersaturation was investigated using two AMSs, a HH-TDMA, two Wyoming static diffusion cloud condensation nuclei (CCN) instruments, a DMT continuous flow CCN instrument, and LACIS.

[54] The structure of the soot particles before coating was found to be of minor importance for the hygroscopic properties and the critical supersaturation of the particles. This is caused by the fact that initially uncompacted soot particles became compacted when a coating was applied [see *Kiselev et al.*, 2010].

[55] Hygroscopic growth and critical supersaturation were calculated based on the soluble mass derived from the AMS via the Köhler equation. This approach works very well for AHSp, LG and even for the more complex particles containing AS, propanol, and LG (ASp&LG), although the AMS measures a particle property that is completely independent from the hygroscopicity/activation. Overall predictions with classical Köhler theory for coated soot based on the number of moles of solute in the coating determined by AMS reproduce the measured GF and S_c relatively well. Maximum deviations were 17% for GF (soot + AHSp) and 30% for S_c for the three component system ASp&LG. For most cases the deviations between the predicted and measured quantities were less than 10%.

[56] The relationship between hygroscopicity and activation was described via two slightly different one-parameter approaches, which avoid unknown properties (e.g., density, molar mass of mixture) in Köhler theory. The resulting closure is excellent for all particles types. This might be explained by the fact that the data included in these approaches (HH-TDMA and CCN) are both direct measures for the particle interaction with water.

[57] Between all accumulated data sets closure is achieved, and this shows a consistent picture of the activation properties of the investigated particles. It also allows an estimate of the cloud-forming potential of combustion particles either directly, through a measurement of CCN activity, or indirectly from hygroscopic growth data or chemical composition measurements. These results may have potential impact for global modeling, especially for CCN activity of biomass burning particles.

[58] **Acknowledgments.** LExNO collaborators whose travel to Leipzig and whose accommodations in Leipzig were supported by ACCENT acknowledge that financial support and wish to thank ACCENT for making their involvement in LExNo a reality. These participants were, in alphabetical order, U. Dusek, G. Frank, A. Kiendler-Scharr, A. Kristensson, T. F. Mentel, D. Rose, J. R. Snider, and S. Walter. M. Bilde and A. Kristensson acknowledge BACCI and FORMAS for support.

References

Albrecht, B. A. (1989), Aerosols, cloud microphysics, and fractional cloudiness, *Science*, *245*, 1227–1230, doi:10.1126/science.245.4923.1227.

Allan, J. D., J. L. Jimenez, P. I. Williams, M. R. Alfarra, K. N. Bower, J. T. Jayne, H. Coe, and D. R. Worsnop (2003), Quantitative sampling using an Aerodyne aerosol mass spectrometer: 1. Techniques of data interpretation and error analysis, *J. Geophys. Res.*, *108*(D3), 4090, doi:10.1029/2002JD002358.

Andreae, M. O., and P. Merlet (2001), Emission of trace gases and aerosols from biomass burning, *Global Biogeochem. Cycles*, *15*, 955–966, doi:10.1029/2000GB001382.

Canagaratna, M. R., et al. (2007), Chemical and microphysical characterization of ambient aerosols with the aerodyne aerosol mass spectrometer, *Mass Spectrom. Rev.*, *26*, 185–222, doi:10.1002/mas.20115.

Dinar, E., et al. (2006), The density of humic acids and humic like substances (HULIS) from fresh and aged wood burning and pollution aerosol particles, *Atmos. Chem. Phys.*, *6*, 5213–5224.

Dusek, U., et al. (2006), CCN activation of pure and coated carbon black particles, *Environ. Sci. Technol.*, *40*, 1223–1230, doi:10.1021/es0503478.

Halstead, W. D. (1970), Thermal decomposition of ammonium sulphate, *J. Appl. Chem.*, *20*, 129–132.

Hennig, T., et al. (2005), A tandem DMA for highly temperature-stabilized hygroscopic particle growth measurements between 90% and 98% relative humidity, *J. Aerosol Sci.*, *36*, 1210–1223, doi:10.1016/j.jaerosci.2005.01.005.

Jayne, J. T., et al. (2000), Development of an aerosol mass spectrometer for size and composition analysis of submicron particles, *Aerosol Sci. Technol.*, *33*, 49–70, doi:10.1080/027868200410840.

Kiselev, A., C. Wennrich, F. Stratmann, H. Wex, S. Henning, T. F. Mentel, A. Kiendler-Scharr, J. Schneider, S. Walter, and I. Lieberwirth (2010), Morphological characterization of soot aerosol particles during LACIS Experiment in November (LExNo), *J. Geophys. Res.*, *115*, D11204, doi:10.1029/2009JD012635.

Kiyoura, R., and K. Urano (1970), Mechanism, kinetics, and equilibrium of thermal decomposition of ammonium sulfate, *Ind. Eng. Chem. Process Des. Dev.*, *9*, 489–494, doi:10.1021/i260036a001.

Koehler, K. A., et al. (2006), Water activity and activation diameters from hygroscopicity data—Part II: Application to organic species, *Atmos. Chem. Phys.*, *6*, 795–809.

Köhler, H. (1936), The nucleus and the growth of hygroscopic droplets, *Trans. Faraday Soc.*, *32*, 1152–1161, doi:10.1039/tf9363201152.

Kütz, S. (1994), In-situ Methoden zur Bestimmung von Struktureigenschaften gasgetragener Agglomerate, Ph.D. thesis, Univ. of Duisburg, Duisburg, Germany.

Lee, Y. S., D. R. Collins, R. Li, K. P. Bowman, and G. Feingold (2006), Expected impact of an aged biomass burning aerosol on cloud condensation nuclei and cloud droplet concentrations, *J. Geophys. Res.*, *111*, D22204, doi:10.1029/2005JD006464.

Low, R. D. H. (1969), A generalized equation for solution effect in droplet growth, *J. Atmos. Sci.*, *26*, 608–610, doi:10.1175/1520-0469(1969)026<0608:AGEFTS>2.0.CO;2.

Mikhailov, E. F., et al. (2001), Interaction of soot aerosol particles with water droplets: Influence of surface hydrophilicity, *J. Aerosol Sci.*, *32*, 697–711, doi:10.1016/S0021-8502(00)00101-4.

Novakov, T., and C. E. Corrigan (1996), Cloud condensation nucleus activity of the organic component of biomass smoke particles, *Geophys. Res. Lett.*, *23*, 2141–2144, doi:10.1029/96GL01971.

Park, Y. J., et al. (1971), The crystal structure of 1, 6-Anhydro-beta-D-glycopyranose, *Acta Crystallogr., Sect. B Struct. Crystallogr. Cryst. Chem.*, *27*, 220–227.

Petters, M. D., and S. M. Kreidenweis (2007), A single parameter representation of hygroscopic growth and cloud condensation nucleus activity, *Atmos. Chem. Phys.*, *7*, 1961–1971.

Roberts, G. C., and A. Nenes (2005), A continuous-flow streamwise thermal-gradient CCN chamber for atmospheric measurements, *Aerosol Sci. Technol.*, *39*, 206–221, doi:10.1080/027868290913988.

Roberts, G. C., A. Nenes, J. H. Seinfeld, and M. O. Andreae (2003), Impact of biomass burning on cloud properties in the Amazon Basin, *J. Geophys. Res.*, *108*(D2), 4062, doi:10.1029/2001JD000985.

Rose, D., et al. (2008), Calibration and measurement uncertainties of a continuous-flow cloud condensation nuclei counter (DMT-CCNC): CCN activation of ammonium sulfate and sodium chloride aerosol particles in theory and experiment, *Atmos. Chem. Phys.*, *8*, 1153–1179.

Rosenorn, T., et al. (2006), Cloud droplet activation of saccharides and levoglucosan particles, *Atmos. Environ.*, *40*, 1794–1802, doi:10.1016/j.atmosenv.2005.11.024.

Schneider, J., et al. (2006), Mass spectrometric analysis and aerodynamic properties of various types of combustion-related aerosol particles, *Int. J. Mass Spectrom.*, *258*, 37–49, doi:10.1016/j.ijms.2006.07.008.

Schultz, M. G., G. A. Heil, J. J. Hoelzemann, A. Spessa, K. Thonicke, J. G. Goldammer, A. C. Held, J. M. C. Pereira, and M. van het Bolscher (2008), Global wildland fire emissions from 1960 to 2000, *Global Biogeochem. Cycles*, *22*, GB2002, doi:10.1029/2007GB003031.

Semeniuk, T. A., et al. (2007), Hygroscopic behavior of aerosol particles from biomass fires using environmental transmission electron microscopy, *J. Atmos. Chem.*, *56*, 259–273, doi:10.1007/s10874-006-9055-5.

Snider, J. R., et al. (2006), Supersaturation in the Wyoming CCN instrument, *J. Atmos. Oceanic Technol.*, *23*, 1323–1339, doi:10.1175/JTECH1916.1.

Snider, J. R., et al. (2010), Intercomparison of cloud condensation nuclei and hygroscopic fraction measurements: Coated soot particles investigated during the LACIS Experiment in November (LExNo), *J. Geophys. Res.*, *115*, D11205, doi:10.1029/2009JD012618.

Stratmann, F., et al. (2004), Laboratory studies and numerical simulations of cloud droplet formation under realistic supersaturation conditions, *J. Atmos. Oceanic Technol.*, *21*, 876–887, doi:10.1175/1520-0426(2004)021<0876:LSANSO>2.0.CO;2.

Stratmann, F., et al. (2010), Examination of laboratory-generated coated soot particles: An overview of the LACIS Experiment in November (LExNo) campaign, *J. Geophys. Res.*, *115*, D11203, doi:10.1029/2009JD012628.

Stroud, C. A., et al. (2007), Cloud activating properties of aerosol observed during CELTIC, *J. Atmos. Sci.*, *64*, 441–459, doi:10.1175/JAS3843.1.

van der Werf, G. R., et al. (2006), Interannual variability in global biomass burning emissions from 1997 to 2004, *Atmos. Chem. Phys.*, *6*, 3423–3441.

Vestin, A., J. Rissler, E. Swietlicki, G. P. Frank, and M. O. Andreae (2007), Cloud-nucleating properties of the Amazonian biomass burning aerosol: Cloud condensation nuclei measurements and modeling, *J. Geophys. Res.*, *112*, D14201, doi:10.1029/2006JD008104.

Wentzel, M., et al. (2003), Transmission electron microscopical and aerosol dynamical characterization of soot aerosols, *J. Aerosol Sci.*, *34*, 1347–1370, doi:10.1016/S0021-8502(03)00360-4.

Wex, H., et al. (2006), Calibration of LACIS as a CCN detector and its use in measuring activation and hygroscopic growth of atmospheric aerosol particles, *Atmos. Chem. Phys.*, *6*, 4519–4527.

Wex, H., T. Hennig, I. Salma, R. Ocskay, A. Kiselev, S. Henning, A. Massling, A. Wiedensohler, and F. Stratmann (2007), Hygroscopic growth and measured and modeled critical super-saturations of an atmospheric HULIS sample, *Geophys. Res. Lett.*, *34*, L02818, doi:10.1029/2006GL028260.

Young, K. C., and A. J. Warren (1992), A reexamination of the derivation of the equilibrium supersaturation curve for soluble particles, *J. Atmos. Sci.*, *49*, 1138–1143, doi:10.1175/1520-0469(1992)049<1138:AROTDO>2.0.CO;2.

Zhang, R. Y., et al. (2008), Variability in morphology, hygroscopicity, and optical properties of soot aerosols during atmospheric processing, *Proc. Natl. Acad. Sci. U. S. A.*, *105*, 10,291–10,296, doi:10.1073/pnas.0804860105.

M. Bilde, Department of Chemistry, University of Copenhagen, Universitetsparken 5, DK-2100 Copenhagen, Denmark.

U. Dusek, Institute for Marine and Atmospheric Research, Utrecht University, Princetonplein 5, NL-3584 CC Utrecht, Netherlands.

G. P. Frank and A. Kristensson, Department of Physics, Lund University, Box 118, SE-22100 Lund, Sweden.

T. Hennig, Institute for Applied Environmental Science, Stockholm University, Svante Arrhenius väg 8, SE-10691 Stockholm, Sweden.

S. Henning, A. Kiselev, F. Stratmann, C. Wennrich, and H. Wex, Institute for Tropospheric Research, Department of Physics, Permoser Str. 15, D-04318, Leipzig, Germany. (silvia.henning@tropos.de)

A. Kiendler-Scharr, T. F. Mentel, and R. Tillmann, ICG-II: Troposphere, Juelich Research Centre, D-52425 Juelich, Germany.

U. Pöschl and D. Rose, Biogeochemistry Department, Max Planck Institute for Chemistry, PO Box 3060, D-55020 Mainz, Germany.

J. Schneider and S. Walter, Particle Chemistry Department, Max Planck Institute for Chemistry, Joh.-Joachim-Becher Weg 27, D-55128 Mainz, Germany.

J. R. Snider, Department of Atmospheric Science, University of Wyoming, Dep. 3038, 1000 E. University Ave., Laramie, WY 82071, USA.